Graphamine: Amine functionalized graphane for intrinsic anhydrous proton conduction

Abhishek Bagusetty,[†,‡] Joshua Livingston,[¶,‡] and J. Karl Johnson[*,‡]

†*Computational Modeling & Simulation Program, University of Pittsburgh, Pittsburgh PA 15260, USA*

‡*Department of Chemical & Petroleum Engineering, University of Pittsburgh, Pittsburgh PA 15261, USA*

¶*New Mexico Tech, Department of Chemical Engineering, Socorro NM 87801, USA*

E-mail: karlj@pitt.edu

Abstract

New proton conducting materials are needed to enable operation of proton exchange membrane fuel cells at intermediate temperatures and conditions of low humidity. We report that graphane functionalized with amine groups (graphamine) can conduct protons in the complete absence of water, as demonstrated by *ab initio* density functional theory molecular dynamics simulations. Graphamine's intrinsic proton conductivity is due to its contiguous network of hydrogen bonds, which facilitate a 'Grotthuss-like' proton hopping mechanism. Our calculations show that graphamine is an electronic insulator having a direct bandgap of 3.08 eV. Our calculated phonon density of states and elastic properties indicate that graphamine is mechanically stable, with an in-plane Young's modulus of 262 J/m^2, which lies in between the values for graphene and graphane. We predict that graphamine has the transport, electronic, and structural properties required for a viable anhydrous proton conduction membrane material.

Proton exchange membrane (PEM) fuel cells are becoming increasingly important for use in applications such as fuel cell electric vehicles and portable power generation.[1] This has lead to a search for more cost-effective and robust materials for proton conduction (PC) to replace Nafion, the current default PC material. One of the main shortcomings of Nafion is that it is not an inherent PC material, i.e., it only conducts protons when hydrated. This leads to problems with water management and results in a relatively narrow window of operating temperatures (< 80°C) for Nafion-based PEM fuel cells. Development of intrinsically PC materials would allow PEM fuel cells to operate over wider temperature ranges, even under anhydrous conditions.[2–4]

New PC materials designed to function under anhydrous or low-humidity conditions include organic polyelectrolytes[5] and crystalline porous materials, such as cucurbituril-based organic molecular porous materials,[6] metal organic frameworks,[7,8] metallopolymers[9] and covalent organic frameworks.[10,11] However, existing materials are subject to a variety of limitations,[8] highlighting the need for development of new PC materials that fulfill all property and cost requirements for PEM fuel cells.

Recently, graphane[12] functionalized with a 1D chain of hydroxyl groups has been shown to exhibit facile PC under anhydrous conditions.[2] The key advantage of hydroxylated graphane compared with other anhydrous PC materials is that the OH groups are covalently bound to the surface with the correct spacing to form a percolating network of hydrogen bonds on the surface, which is required for rapid anhydrous PC. Moreover, this network is relatively rigid, meaning that thermal fluctuations do not disrupt the hydrogen bonding network as much as in more flexible materials, such as polymers. Given these features, we seek to identify other functional derivatives of graphane for robust anhydrous PC. In this work, we examine surface functionalization of chair graphane with amine groups ($–NH_2$) as a potential anhydrous PC material. The objectives of this paper are to: (1) test whether amine-functionalized graphane (graphamine) can conduct protons under anhydrous conditions, (2) estimate the bandgap of graphamine, and (3) explore the mechanical properties of graphamine. The bandgap is of

interest because any practical PEM material must be electrically insulating to avoid short circuiting the fuel cell. Good mechanical properties are required for constructing robust fuel cell stacks. We here report density functional theory (DFT) calculations predicting the PC, electronic, and mechanical properties of graphamine.

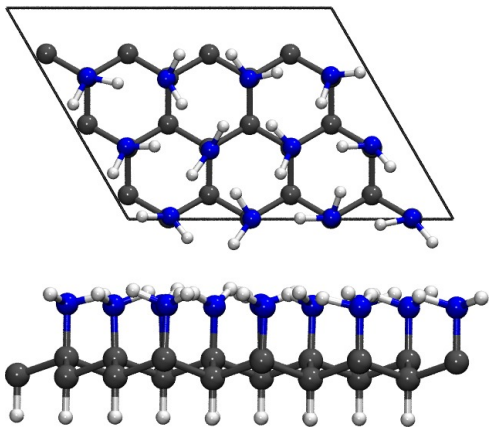

Figure 1: Schematic representation of top and side view of a graphamine (4×3) supercell (carbons in gray, nitrogens in blue, hydrogens in white). Solid lines show the supercell boundaries in the $\vec{a}$ and $\vec{b}$ directions.

All the AIMD simulations were performed using the Quickstep module[13] in the CP2K package.[14] The Perdew-Burke-Ernzerhof (PBE)[15] exchange correlation functional was used, along with a hybrid Gaussian and plane waves method,[16] employing DZVP-MOLOPT basis sets[17] with GTH pseudopotentials.[18] A plane wave energy cutoff of 440 Ry and relative cutoff of 40 Ry. The orbital transformation method[19] was used to optimize the wave functions at each step of the simulations. AIMD simulations within the *NVT* (canonical) ensemble were performed for thermal equilibration using colored-noise GLE thermostat.[20,21] A time step of 0.5 fs for integration under Γ point sampling of the Brillouin zone was employed. A set of five independent *NVE* (microcanonical) ensemble simulations were performed starting from initial configurations (positions and velocities) obtained from thermalized *NVT* simulations. The *NVE* AIMD simulations were run for 30 ps for data collection.

Electronic and mechanical properties (phonon density of states and elastic constants) require a higher level of accuracy than PC dynamics calculations; we have therefore carried

out these calculations using the Vienna *Ab initio* Simulation Package (VASP).[22–24] Projector augmented-wave pseudopotentials[25] were employed to describe the interactions between valence electrons and frozen cores. A kinetic energy cutoff for the plane-wave expansion of 520 eV was used. We used the Perdew-Burke-Ernzerhof (PBE)[15] generalized gradient approximation (GGA) exchange-correlation functional for the structural and mechanical calculations. The structural relaxation and lattice properties (a = 10.703 Å, b = 8.027 Å, c = 20.0 Å, α=β=90°, γ=120°) for the supercell shown in Figure 1 were computed on a 7 × 7 × 1 **k** point grid. The energies were converged to within 10^{-9} eV and the ionic positions were optimized until the forces were converged to less than 10^{-3} eV/Å. A vacuum spacing of 20 Å in the $\vec{c}$ direction was used to mitigate the periodic interactions. Harmonic phonon dispersion calculations were computed at the PBE level of theory using Phonopy.[26] We used a 3 × 3 × 1 supercell of the configuration shown in Figure 1 for the phonon calculations.

Our DFT calculations were carried out using a 4 × 3 supercell of a single layer of graphamine, as shown in Figure 1 (see Supporting Information for atomic coordinates). Graphamine was constructed by replacing the surface H atoms on one side of graphane with amine groups. As a result of functionalization, the C–C bond length increases from 1.54 Å[27] to 1.62 Å. Alternately, one could completely functionalize both sides of graphane, producing a fully saturated graphamine to increase the overall conduction. We employed *ab initio* molecular dynamics (AIMD) simulations performed at a temperature of about 1000 K in the constant energy (microcanonical) ensemble to estimate the thermodynamic stability and proton diffusivity of graphamine having one additional proton per supercell, such that the system has a +1 e charge. It is well known that periodic DFT calculations of charged systems are problematic because of the errors due to imposing an artificial jellium background.[28] However, Bagusetty et al. have shown that no significant errors arise for computing PC on hydroxylated graphane.[2] We therefore do not apply any charge-based corrections in this work.

Proton Conduction Dynamics. An analysis of the AIMD simulations showed that PC

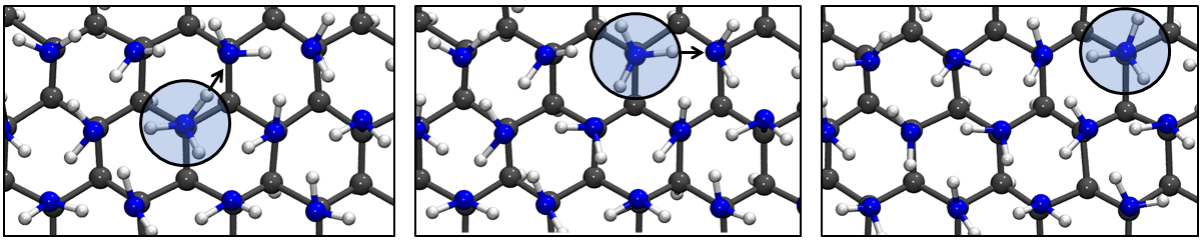

Figure 2: Snapshots from an AIMD simulation showing an example of a Grotthuss-like proton conduction event. The system contains one excess proton and the charge center is marked with the shaded circle in each snapshot. The direction of the proton hop is indicated by the arrow (colors are defined in Figure 1).

occurs through proton hopping along the 2-D hydrogen bonding network of graphamine, accompanied by rotation of NH_2 groups. Given the morphology of graphamine, the protons are transported by hopping between adjacent amine groups in a Grotthuss-like mechanism,[29] facilitated by hydrogen bonding between neighboring amine groups. The average number of hydrogen bonds (donor and acceptor) per NH_2 group is about 3, as computed from a distance-based criterion. Hydrogen bonds were determined based on a geometric distance criterion of an N—H distance $\leq$ 2.7 Å for non-bonded atoms.[30] Hydrogen bond distance data and PC events were collected from AIMD trajectories at 1000 K.

An example of a proton hopping event obtained from snapshots from an AIMD simulation is shown in Figure 2, from which one can observe only slight reorientation of the neighboring amine groups as a result of the hopping event. We have computed mean square displacements (MSD) of all H atoms bound to N atoms from AIMD simulations at about 1000 K for the graphamine system with one proton. The plot of MSD/t, where t is time is shown in Figure 3. The flat profile (MSD/t = constant at large values of t) is a signature of Fickian diffusion, i.e., $dr^2 \propto Ddt$ where D is the Fickian diffusion coefficient.[31] The diffusion coefficient at 1000 K, estimated from the Einstein relation ($D = \lim_{t\to\infty}\langle|r(t)-r(0)|^2\rangle/(2dt)$, where $d = 2$ is the dimensionality of the system) is 1.62×10^{-5} cm^2/s. For comparison, simulations of PC in Nafion at room temperature give D in the range of 1.4×10^{-6} cm^2/s to 1.7×10^{-5} cm^2/s, depending on the level of hydration.[32] We note that proton diffusivity in Nafion drops dramatically above about 80° C because of the loss of water from the membrane.

We observed from AIMD simulations that the PC mechanism involves a proton moving from the —NH_3 group to a neighboring —NH_2 group, as seen if Figure 2. One might reasonably assume that one or more of the H atoms on the —NH_3 group would have a significantly larger charge than the H atoms on the —NH_2 groups on the graphamine surface. In other words, it seems reasonable to assume that the center of charge would be highly localized. We have checked this assumption by computing the charge distribution on the H atoms bound to N atoms for the system with a single proton using the Density Derived Electrostatic and Chemical (DDEC6) charge analysis approach.[33] However, our DDEC6 calculations show that the charge is highly delocalized (see charge analysis in Figure S2 and Tables S2 and S3 of the Supporting Information). The largest value of the charge is 0.287 e, and while it does belong to an H atom on the —NH_3 group, this value is only slightly larger than the next largest charge of 0.277 e, which is on an —NH_2 group. The mean charge on all H atoms bound to N is 0.257 e and the standard deviation is 0.013 e. This indicates that the charge center is delocalized, even though graphamine is a wide bandgap semiconductor (as shown below).

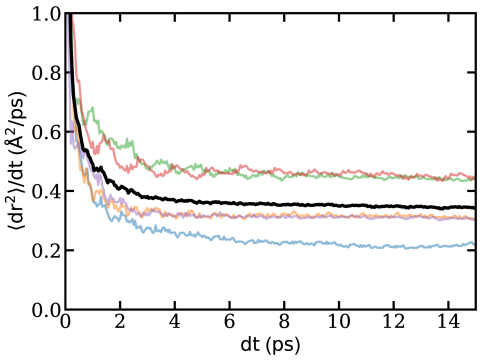

Figure 3: Plots of the mean square displacements divided by time of all the H atoms bound to N atoms on the graphamine surface having one proton. Plots for five independent runs are shown in various colors and the average of the five runs is shown as the thick black curve. The average temperature of the simulations was about 1000 K.

Mechanical and Electronic Properties. Having established that graphamine has the ability to conduct protons under anhydrous conditions, we turn to questions of whether it has suitable electronic and mechanical properties for a PEM material. Specifically, PEM materials

must be electrically insulating and mechanically robust.

Chemical functionalization of sp^3 hybridized graphane to form aminated graphane gives a C—N covalent bond length of 1.48 Å in comparison to the semi-ionic C—N bond length of 1.518 Å reported for amine functionalized graphene.[34] The hydrogens of the amine groups in graphamine tend to orient roughly towards the centers of the underlying graphane hexagons rather than to align with the C—C bonds, as seen in Figure 1. The average H—N—H bend angle is 107.8°, as computed for the configuration in Figure 1. An analysis of the hydrogen bonds gave a mean N—H and N—N hydrogen bond distance of 2.2(±0.32) and 2.68(±0.08) Å, respectively. In comparison, hydrogen bonding distances for N—H and N—N in liquid ammonia are reported to be 2.7 and 3.35 Å, respectively.[30] The shorter hydrogen bonding donor-acceptor distances observed in graphamine compared to liquid ammonia, coupled with the observation that the NH_2 groups on graphamine can rotate (as seen from AIMD simulations) indicate that proton transfer should be more facile on graphamine than in liquid ammonia.

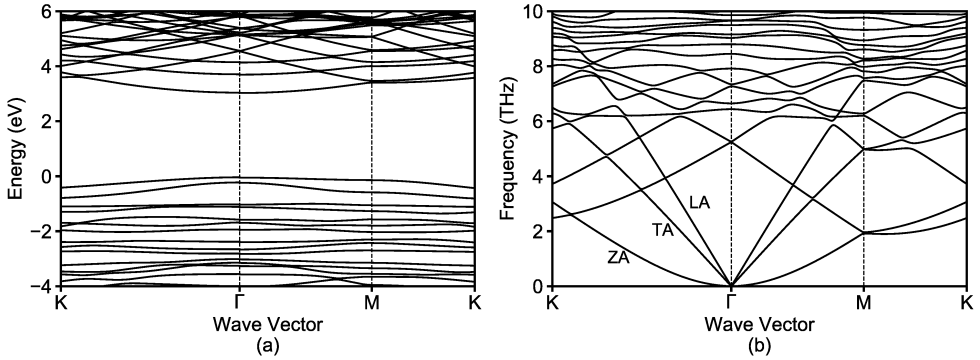

Figure 4: (a) HSE06 band structure of graphamine along high-symmetry paths showing a direct bandgap of 3.08 eV. The Fermi level is shifted to zero energy. (b) Phonon dispersion curves calculated for graphamine.

Electronic Band Structure. Graphane is a wide bandgap material with a direct bandgap of 3.5 eV as estimated from GGA for the ground state chair conformation.[35] Functionalization of graphane can reduce the bandgap; it has been reported that introducing a hydroxyl group defect by the replacement of an H atom in a 3 × 3 graphane supercell reduces the GGA

bandgap to 3.3 eV.[35] Replacing all the H atoms on one surface of graphane with hydroxyl groups gives a material with an estimated bandgap of 3.22 eV.[36] Given these trends, we expect that the bandgap of graphamine will be reduced with respect to graphane. We employed the Heyd-Scuseria-Ernzerhorf (HSE06) hybrid functional[37] to obtain an accurate band structure because it is well-known that the GGA formalism generally underestimates the bandgap of semiconductors. We have computed the band structure of graphamine using both the PBE and hybrid HSE06 functionals. Both methods predict that graphamine is a wide-bandgap semiconductor with a direct gap at the Γ point. The PBE bandgap is 2.04 eV while the screened-hybrid HSE06 functional, which predicts accurate bandgaps for typical semiconductors,[38] gives a gap of 3.08 eV. The HSE06 band structure plot is shown in Figure 4(a). These calculations indicate that graphamine has an appropriate bandgap to be used as a PEM material.

Phonon and Elastic Properties. We have computed the phonon dispersion curves for graphamine in order to estimate its stability. The curves are plotted in Figure 4(b). The absence of soft modes (modes with imaginary frequencies) along any high-symmetry direction of the Brillouin zone indicates that there are no instabilities in graphamine, within the harmonic approximation. Only the lower frequency dispersion branches with values less than 10 THz are shown in Figure 4(b) in order to focus on the acoustic modes along principle directions (the full phonon dispersion spectrum in shown in Figure S3 of the Supporting Information). The longitudinal acoustic LA and transverse acoustic TA branches show linear profiles, while the out of plane acoustic ZA modes show quadratic dispersion. This is very similar to the behavior observed for graphene and its layered derivatives.[39] We have also calculated the phonon density of states, shown in Figure S3 of the Supporting Information.

We performed calculations for the elastic properties under harmonic strain limits ($\epsilon < \pm$ 2%) by applying uniaxial and equi-biaxial in-plane strain. Calculation of in-plane Young's modulus, (Y) and Poisson's ratio, (ν), are estimated from elastic constants C_{11} and C_{12}

related by the expressions,

$$Y = \frac{C_{11}^2 - C_{12}^2}{C_{11}} \tag{1}$$

$$\nu = \frac{C_{12}}{C_{11}} \tag{2}$$

A rectangular supercell was used for these calculations (shown in Figure S4 of the Supporting Information). A set of 20 lattice parameters were obtained by perturbing the equilibrium lattice parameters accordingly to reflect compression and tension. The atomic positions were then scaled to accommodate the new lattice parameters and the atoms were allowed to fully relax until the energy convergence tolerance of 10^{-8} eV. The elastic strain energy (E_s) per unit area was determined as a difference between electronic energy under strain ($E_s(\epsilon)$) and system at equilibrium ($E_s(\epsilon = 0)$). Under uniaxial conditions, strain was applied only along x-direction ($\epsilon_{yy} = 0$) and strain energy was fit to a parabolic expression $E_s(\epsilon_{xx}) = C_{11}\epsilon_{xx}^2/2$. Similarly, equi-biaxial ($\epsilon_{xx} = \epsilon_{yy}$) strain energy was fit to an expression $E_s(\epsilon_{xx}) = (C_{11} + C_{12})\epsilon_{xx}^2$ (details on the fit are presented in Figure S5 of the Supporting Information). The calculated value of Y is 262 J/m^2, which falls in between the reported values for chair graphane (243 J/m^2)[27,40] and graphene (340 $\pm$ 50 J/m^2).[41] The reduction of the in-plane Young's modulus for chair graphane relative to graphene is the result of sp^3 hybridization, which makes graphane easier to deform under loading compared to sp^2 hybridized graphene. Our calculations show that functionalization of graphane with amine groups yields a higher value of Y compared to graphane because the hydrogen bonded network of amine groups provides additional resistance to applied strain. Hence, there should be an opportunity to tune Y to a certain degree through control of the degree of functionalization. We note that our results are for graphamine with a single side functionalized with amine groups. We predict that functionalization of both sides of graphane with amine groups will produce an even larger value of Y. The value of Poisson's ratio was determined to be 0.13, which is close to the values reported for graphene (0.16)[41] and almost double than chair graphane (0.07).[40]

An observed increase in the value of ν compared to chair graphane can be attributed to the formation of a 2-D network of hydrogen bonding layer from amine groups. This dense network of hydrogen bonds provides resistance to longitudinal elongation thus increasing the value of ν.

In summary, we have predicted that graphamine is a promising PEM material for facilitating PC under anhydrous and low-humidity conditions. Graphamine has a contiguous network of hydrogen bonds that are much closer than in liquid ammonia. This compressed hydrogen bonding network, coupled with the ability of the —NH_2 groups to rotate, facilitates PC in the compete absence of water, as seen from our AIMD simulations. We have shown that graphamine is a wide bandgap semiconductor, having a direct gap of 3.08 eV. The phonon density of states and dispersion relations indicate that graphamine is mechanically stable. Additionally, it has an in-plane Young's modulus larger than unfunctionalized graphane; we predict that the in-plane Young's modulus can be tuned by functionalization of graphane. We note that amine functionalized graphene oxide has been experimentally synthesized,[42–47] but that fully aminated graphane has not yet been produced. Our work provides motivation for synthesis and characterization of more uniformly functionalized graphamine.

The Supporting Information is available free of charge on the ACS Publications website. Atomic coordinates, additional computational details, DDEC6 partial charge analysis and phonon dispersion for graphamine.

Acknowledgement

This work was supported by the National Science Foundation under Award No. CBET 1703266. Computations were carried out with support from the Extreme Science and Engineering Discovery Environment (XSEDE) of National Science Foundation under allocation No. TG-DMR110091 and the Center for Research Computing at the University of Pittsburgh.

References

(1) Wee, J.-H. Applications of proton exchange membrane fuel cell systems. Renew. Sust. Energy. Rev. **2007**, 11, 1720–1738.

(2) Bagusetty, A.; Choudhury, P.; Saidi, W. A.; Derksen, B.; Gatto, E.; Johnson, J. K. Facile Anhydrous Proton Transport on Hydroxyl Functionalized Graphane. Phys. Rev. Lett. **2017**, 118, 186101.

(3) Nagarkar, S. S.; Unni, S. M.; Sharma, A.; Kurungot, S.; Ghosh, S. K. Two-in-One: Inherent Anhydrous and Water-Assisted High Proton Conduction in a 3D Metal-Organic Framework. Angew. Chem. **2013**, 126, 2676.

(4) Schuster, M. F.; Meyer, W. H. Anhydrous Proton conducting polymers. Annu. Rev. Mater. Sci. **2003**, 33, 233–261.

(5) Paddison, S. Proton Conduction Mechanisms at Low Degrees of Hydration in Sulfonic Acid-Based Polymer Electrolyte Membranes. Annu. Rev. Mater. Sci. **2003**, 33, 289.

(6) Yoon, M.; Suh, K.; Kim, H.; Kim, Y.; Selvapalam, N.; Kim, K. High and Highly Anisotropic Proton Conductivity in Organic Molecular Porous Materials. Angew. Chem. Int. Ed. **2011**, 50, 7870–7873.

(7) Shimizu, G. K. H.; Taylor, J. M.; Kim, S. Proton Conduction with Metal-Organic Frameworks. Science **2013**, 341, 354.

(8) Ramaswamy, P.; Wong, N. E.; Shimizu, G. K. H. MOFs as proton conductors– challenges and opportunities. Chem. Soc. Rev. **2014**, 43, 5913.

(9) Chakraborty, C.; Rana, U.; Pandey, R. K.; Moriyama, S.; Higuchi, M. One-Dimensional Anhydrous Proton Conducting Channel Formation at High Temperature in a Pt(II)-Based Metallo-Supramolecular Polymer and Imidazole System. ACS Appl. Mater. Interfaces **2017**, 9, 13406.

(10) Chandra, S.; Kundu, T.; Kandambeth, S.; BabaRao, R.; Marathe, Y.; Kunjir, S. M.; Banerjee, R. Phosphoric Acid Loaded Azo (−N = N−) Based Covalent Organic Framework for Proton Conduction. J. Am. Chem. Soc. **2014**, 136, 6570.

(11) Peng, Y.; Xu, G.; Hu, Z.; Cheng, Y.; Chi, C.; Yuan, D.; Cheng, H.; Zhao, D. Mechanoassisted Synthesis of Sulfonated Covalent Organic Frameworks with High Intrinsic Proton Conductivity. ACS Appl. Mater. Interfaces **2016**, 8, 18505.

(12) Sofo, J. O.; Chaudhari, A. S.; Barber, G. D. Graphane: A two-dimensional hydrocarbon. Phys. Rev. B **2007**, 75, 153401.

(13) VandeVondele, J.; Krack, M.; Mohamed, F.; Parrinello, M.; Chassaing, T.; Hutter, J. Quickstep: Fast and Accurate Density Functional Calculations Using a Mixed Gaussian and Plane Waves Approach. Comput. Phys. Commun. **2005**, 167, 103–128.

(14) Hutter, J.; Iannuzzi, M.; Schiffmann, F.; VandeVondele, J. CP2K: Atomistic Simulations of Condensed Matter Systems. WIREs Comput Mol Sci. **2013**, 4, 15–25.

(15) Perdew, J. P.; Burke, K.; Ernzerhof, M. Generalized Gradient Approximation Made Simple. Phys. Rev. Lett. **1996**, 77, 3865–3868.

(16) Lippert, G.; Hutter, J.; Parrinello, M. The Gaussian and Augmented-Plane-Wave Density Functional Method for Ab Initio Molecular Dynamics Simulations. Theor. Chem. Acc. **1999**, 103, 124–140.

(17) VandeVondele, J.; Hutter, J. Gaussian Basis Sets for Accurate Calculations on Molecular Systems in Gas and Condensed Phases. J. Chem. Phys. **2007**, 127, 114105.

(18) Goedecker, S.; Teter, M.; Hutter, J. Separable Dual-Space Gaussian Pseudopotentials. Phys. Rev. B **1996**, 54, 1703–1710.

(19) VandeVondele, J.; Hutter, J. An Efficient Orbital Transformation Method for Electronic Structure Calculations. J. Chem. Phys. **2003**, 118, 4365.

(20) Ceriotti, M.; Bussi, G.; Parrinello, M. Nuclear Quantum Effects in Solids Using a Colored-Noise Thermostat. Phys. Rev. Lett. **2009**, 103, 030603.

(21) Ceriotti, M.; Bussi, G.; Parrinello, M. Langevin Equation with Colored Noise for Constant-Temperature Molecular Dynamics Simulations. Phys. Rev. Lett. **2009**, 102, 020601.

(22) Kresse, G.; Hafner, J. Ab Initio Molecular Dynamics for Liquid Metals. Phys. Rev. B **1993**, 47, 558–561.

(23) Kresse, G.; Furthmüller, J. Efficient Iterative Schemes for Ab Initio Total-Energy Calculations Using a Plane-Wave Basis Set. Phys. Rev. B **1996**, 54, 11169–11186.

(24) Kresse, G.; Furthmüller, J. Efficiency of Ab-Initio Total Energy Calculations for Metals and Semiconductors Using a Plane-Wave Basis Set. Comput. Mater. Sci. **1996**, 6, 15–50.

(25) Kresse, G.; Joubert, D. From Ultrasoft Pseudopotentials To the Projector Augmented-Wave Method. Phys. Rev. B **1999**, 59, 1758–1775.

(26) Togo, A.; Tanaka, I. First principles phonon calculations in materials science. Scr. Mater. **2015**, 108, 1–5.

(27) Cadelano, E.; Palla, P. L.; Giordano, S.; Colombo, L. Elastic properties of hydrogenated graphene. Phys. Rev. B **2010**, 82, 235414.

(28) Makov, G.; Payne, M. C. Periodic Boundary Conditions in Ab Initio Calculations. Phys. Rev. B **1995**, 51, 4014–4022.

(29) Agmon, N. The Grotthuss mechanism. Chemical Physics Letters **1995**, 244, 456–462.

(30) Boese, A. D.; Chandra, A.; Martin, J. M. L.; Marx, D. From ab initio quantum chemistry to molecular dynamics: The delicate case of hydrogen bonding in ammonia. J. Chem. Phys. **2003**, 119, 5965–5980.

(31) Striolo, A. The Mechanism of Water Diffusion in Narrow Carbon Nanotubes. Nano Lett. **2006**, 6, 633.

(32) Feng, S.; Voth, G. A. Proton Solvation and Transport in Hydrated Nafion. J. Phys. Chem. B **2011**, 115, 5903–5912.

(33) Limas, N. G.; Manz, T. A. Introducing DDEC6 Atomic Population Analysis: Part 2. Computed Results for a Wide Range of Periodic and Nonperiodic Materials. RSC Adv. **2016**, 6, 45727.

(34) Junkermeier, C. E.; Solenov, D.; Reinecke, T. L. Adsorption of NH2 on Graphene in the Presence of Defects and Adsorbates. J. Phys. Chem. C **2013**, 117, 2793.

(35) Lebègue, S.; Klintenberg, M.; Eriksson, O.; Katsnelson, M. I. Accurate Electronic Band Gap of Pure and Functionalized Graphane From GW Calculations. Phys. Rev. B **2009**, 79, 245117.

(36) Wang, W. L.; Kaxiras, E. Graphene Hydrate: Theoretical Prediction of a New Insulating Form of Graphene. New J. Phys. **2010**, 12, 125012.

(37) Heyd, J.; Scuseria, G. E.; Ernzerhof, M. Hybrid functionals based on a screened Coulomb potential. J. Chem. Phys. **2003**, 118, 8207.

(38) Garza, A. J.; Scuseria, G. E. Predicting Band Gaps with Hybrid Density Functionals. J. Phys. Chem. Lett **2016**, 7, 4165.

(39) Mounet, N.; Marzari, N. First-principles determination of the structural, vibrational and thermodynamic properties of diamond, graphite, and derivatives. Phys. Rev. B **2005**, 71, 205214.

(40) Topsakal, M.; Cahangirov, S.; Ciraci, S. The Response of Mechanical and Electronic Properties of Graphane To the Elastic Strain. Appl. Phys. Lett. **2010**, 96, 091912.

(41) Lee, C.; Wei, X.; Kysar, J. W.; Hone, J. Measurement of the Elastic Properties and Intrinsic Strength of Monolayer Graphene. Science **2008**, 321, 385.

(42) Ederer, J.; Janoš, P.; Ecorchard, P.; Tolasz, J.; Štengl, V.; Beneš, H.; Perchacz, M.; Pop-Georgievski, O. Determination of amino groups on functionalized graphene oxide for polyurethane nanomaterials: XPS quantitation vs. functional speciation. RSC Adv. **2017**, 7, 12464–12473.

(43) Sandoval, S.; Kumar, N.; Oro-Solé, J.; Sundaresan, A.; Rao, C.; Fuertes, A.; Tobias, G. Tuning the nature of nitrogen atoms in N-containing reduced graphene oxide. Carbon **2016**, 96, 594 – 602.

(44) Zhang, W.; Ma, J.; Gao, D.; Zhou, Y.; Li, C.; Zha, J.; Zhang, J. Preparation of amino-functionalized graphene oxide by Hoffman rearrangement and its performances on polyacrylate coating latex. Prog. Org. Coat **2016**, 94, 9 – 17.

(45) Khai, T. V.; Na, H. G.; Kwak, D. S.; Kwon, Y. J.; Ham, H.; Shim, K. B.; Kim, H. W. Influence of N-doping on the structural and photoluminescence properties of graphene oxide films. Carbon **2012**, 50, 3799 – 3806.

(46) Lai, L.; Chen, L.; Zhan, D.; Sun, L.; Liu, J.; Lim, S. H.; Poh, C. K.; Shen, Z.; Lin, J. One-step synthesis of NH2-graphene from in situ graphene-oxide reduction and its improved electrochemical properties. Carbon **2011**, 49, 3250 – 3257.

(47) Liu, P.; Wang, H.; Yan, T.; Zhang, J.; Shi, L.; Zhang, D. Grafting sulfonic and amine functional groups on 3D graphene for improved capacitive deionization. J. Mater. Chem. A **2016**, 4, 5303–5313.

Graphical TOC Entry